

Article

Excellent Magnetocaloric Performance of the $\text{Fe}_{87}\text{Ce}_{13-x}\text{B}_x$ ($x = 5, 6, 7$) Metallic Glasses and Their Composite

Shu-Hui Zheng ¹, Qiang Wang ¹ , Li-Ze Zhu ¹, Peng-Jie Wang ¹, Ding Ding ¹ , Ben-Zhen Tang ², Peng Yu ² , Jin-Lei Yao ³ and Lei Xia ^{1,*} 

- ¹ Institute of Materials & Laboratory for Microstructure, Shanghai University, Shanghai 200072, China; zhengshuhui@shu.edu.cn (S.-H.Z.); mat_wq@shu.edu.cn (Q.W.); lize_zhu@163.com (L.-Z.Z.); w_pengjie@163.com (P.-J.W.); d.ding@shu.edu.cn (D.D.)
- ² Chongqing Key Laboratory of Photo-Electric Functional Materials, College of Physics and Electronic Engineering, Chongqing Normal University, Chongqing 401331, China; bz.tang@cqnu.edu.cn (B.-Z.T.); pengyu@cqnu.edu.cn (P.Y.)
- ³ Jiangsu Key Laboratory of Micro and Nano Heat Fluid Flow Technology and Energy Application, School of Physical Science and Technology, Suzhou University of Science and Technology, Suzhou 215009, China; jlyao@usts.edu.cn
- * Correspondence: xialei@shu.edu.cn; Tel.: +86-021-6613-5067

Abstract: The novel $\text{Fe}_{87}\text{Ce}_{13-x}\text{B}_x$ ($x = 5, 6, 7$) metallic glass (MG) ribbons were fabricated in this work. The compositional dependence of glass forming ability (GFA), magnetic and magnetocaloric properties of these ternary MGs, and the mechanism involved was investigated. The GFA and Curie temperature (T_c) of the MG ribbons were found to improve with the boron content, and the peak value of magnetic entropy change ($-\Delta S_m^{\text{peak}}$) reaches a maximum of 3.88 J/(kg \times K) under 5 T when $x = 6$. Based on the three results, we designed an amorphous composite that exhibits a table-shape magnetic entropy change ($-\Delta S_m$) profile with a rather high average $-\Delta S_m$ ($-\Delta S_m^{\text{average}} \sim 3.29$ J/(kg \times K) under 5 T) from 282.5 K to 320 K, which makes it a potential candidate for the highly efficient refrigerant in a domestic magnetic refrigeration appliance.

Keywords: metallic glass; glass-forming ability; Curie temperature; table-like magnetic entropy change profile



Citation: Zheng, S.-H.; Wang, Q.; Zhu, L.-Z.; Wang, P.-J.; Ding, D.; Tang, B.-Z.; Yu, P.; Yao, J.-L.; Xia, L. Excellent Magnetocaloric Performance of the $\text{Fe}_{87}\text{Ce}_{13-x}\text{B}_x$ ($x = 5, 6, 7$) Metallic Glasses and Their Composite. *Materials* **2023**, *16*, 4393. <https://doi.org/10.3390/ma16124393>

Academic Editor: E. Andrew Payzant

Received: 13 May 2023
Revised: 5 June 2023
Accepted: 13 June 2023
Published: 14 June 2023



Copyright: © 2023 by the authors. Licensee MDPI, Basel, Switzerland. This article is an open access article distributed under the terms and conditions of the Creative Commons Attribution (CC BY) license (<https://creativecommons.org/licenses/by/4.0/>).

1. Introduction

Recently, the demand for refrigeration has risen sharply because of the ongoing and extremely high-temperature weather. However, conventional refrigeration technology can make this problem worse due to the generation of ozone-depleting gases by refrigerants. A novel refrigeration technology, namely magnetic refrigeration (MR, which has the advantages of high efficiency, environmental friendliness, great stability and reliability, low noise, and easy miniaturization [1–5]), may be a better choice. The MR technology was first used by Gauque in 1933 to achieve ultra-low temperatures below 1 K and has been applied to the low and medium temperature regions up to now [6,7], although it is still in the research stage at high temperatures, especially for civil applications at room temperature. One of the key issues affecting the civil application of MR is the magnetocaloric effect (MCE) performance of refrigerants.

Although a large number of compounds with ultrahigh magnetic entropy change ($-\Delta S_m$) have been developed, their narrow working temperature ranges make them difficult to synthesize a composite material with a flattened $-\Delta S_m$ curve [8–11], which is of great significance for the optimization of cooling efficiency in the Ericsson cycle [12]. Additionally, the presence of magnetic hysteresis and thermal hysteresis in these compounds prevents them from operating at high frequencies with fast response. On the contrary, the metallic glasses (MGs) that exhibit a broader $-\Delta S_m$ peak ($-\Delta S_m^{\text{peak}}$) without magnetic hysteresis and thermal hysteresis are preferred, such as Gd-based and Fe-based MGs [13–26].

The tunable Curie temperature (T_c) in a wide range of composition adjustments is beneficial for constructing the flattened $-\Delta S_m$ curve [15–17]. Furthermore, the advantages of outstanding mechanical, physical, and chemical properties can also ensure that MGs have a longer service life and numerous application scenarios [27,28]. For example, Zr-based or Ti-based MGs with both ultra-high strength and plasticity have made significant progress in key structural materials for military and aerospace equipment; Ca-based, Mg-based, or Fe-based MGs possess good biocompatibility and comprehensive mechanical properties and are expected to be used in artificial bones.

Compared with rare-earth (RE)-based MGs, Fe-based MGs show greater application value in civil aspects (such as magnetic refrigerators, air conditioners, wine cabinets, and so on) due to their lower cost and better glass forming ability (GFA), but the $-\Delta S_m^{peak}$ of these Fe-based MGs is not as high as that of RE-based MGs [15–26]. Therefore, improving the $-\Delta S_m^{peak}$ of the Fe-based MGs as much as possible is a top priority for the civil application of MR technology. Amongst these reported Fe-based MGs, Fe-Zr-B-based MG ribbons are the outstanding ones [15–18,23–26]. For example, the Fe-Zr-B ternary amorphous ribbons exhibited a $-\Delta S_m^{peak}$ under 5 T of 2.75–3.34 J/(kg \times K) at the T_c ranging from 271 K to 327 K [18,24]. By minor element substitution, the $-\Delta S_m^{peak}$ under 5 T of the multicomponent Fe-Zr-B-based MG ribbons was increased to a maximum value of 3.55 J/(kg \times K) at 336 K [26]. Unfortunately, the values of $-\Delta S_m^{peak}$ in these Fe-Zr-B-based MG ribbons are still not as high for the practical application of MR. In our recent works, we found that Fe-La/Ce-B-based glassy ribbons show rather excellent MCE near room temperature, and the $-\Delta S_m^{peak}$ under 5 T of Fe₈₇Ce₈B₅ ribbon reaches 3.65 J/(kg \times K) at 283 K, which is 12.3% higher than that of Fe₈₇Zr₈B₅ metallic glass and exceeds the $-\Delta S_m^{peak}$ of most other Fe-Zr-B-based amorphous alloys [29,30]. The large $-\Delta S_m^{peak}$ of the Fe₈₇Ce₈B₅ amorphous ribbon was attributed to the extra magnetic moment of the Ce atom, but the effect of Ce content on the $-\Delta S_m^{peak}$ of the Fe-Ce-B MG ribbons and the involved mechanism is still unclear. The detailed investigation of the magnetic and magnetocaloric properties of the Fe-Ce-B ternary MG ribbons will be helpful for the clarification of the effects of the Ce content on the magnetic properties and MCE of the Fe-Ce-B MG ribbons and the further development of the multicomponent Fe-based amorphous alloys with better MCE near room temperature. As such, we prepared the Fe₈₇Ce_{13-x}B_x ($x = 5, 6, 7$) amorphous ribbons using melt-spinning technology and systematically investigated the influences of boron on GFA, T_c and $-\Delta S_m^{peak}$ of the three ribbons, as well as the mechanisms involved, in this paper. Finally, an amorphous composite with a flattened $-\Delta S_m$ profile was designed according to the three samples.

2. Materials and Methods

The Fe₈₇Ce_{13-x}B_x ($x = 5, 6, 7$) alloy ingots were prepared by melting high-purity raw materials (≥ 99.9 at%) using a vacuum arc-melting furnace with the protection of Ar gas. Each ingot of the Fe₈₇Ce_{13-x}B_x ($x = 5, 6, 7$) master alloys was melted more than four times to ensure their compositional homogeneity. These ingots were remelted in a quartz tube again and sprayed onto the surface of a high-speed (~ 55 m/s) rotating copper roller to form the Fe₈₇Ce_{13-x}B_x ($x = 5, 6, 7$) ribbons. The structure of these ribbons was characterized by a PANalytical X-ray diffractometer with Cu K_α radiation. The differential scanning calorimetry (DSC) traces were measured at a heating rate of 20 K/min on a Netzsch DSC 404C calorimeter to evaluate the GFA of the Fe₈₇Ce_{13-x}B_x ($x = 5, 6, 7$) ribbons. The magnetic measurements of the samples, including hysteresis loops, magnetization vs. temperature (M - T) curves, and isothermal magnetization (M - H) curves, were performed on a vibrating sample magnetometer (VSM), which is a module of 6000 Physical Property Measurement System (PPMS, Quantum Design).

3. Results and Discussion

Figure 1a shows the XRD patterns of the Fe₈₇Ce_{13-x}B_x ($x = 5, 6, 7$) ribbons. Only smooth diffraction humps between 40° and 50° and no obvious crystalline peaks were

observed in these patterns, indicating the amorphous structure of the $\text{Fe}_{87}\text{Ce}_{13-x}\text{B}_x$ ($x = 5, 6, 7$) ribbons. Figure 1b displays the DSC curves of the $\text{Fe}_{87}\text{Ce}_{13-x}\text{B}_x$ ($x = 5, 6, 7$) amorphous ribbons. A weak glass transition endothermic hump before a sharp crystallization exothermic peak was found in each DSC curve, which further confirms the glassy characteristics of the three ribbons. From their DSC curves, we can obtain the thermal parameters, including the onset temperature of glass transition (T_g^{onset}) and crystallization (T_x^{onset}), and liquidus temperature (T_l), of the $\text{Fe}_{87}\text{Ce}_{13-x}\text{B}_x$ ($x = 5, 6, 7$) MG ribbons, as listed in Table 1. As a result, the reduced glass transition temperature ($T_{rg} = T_g/T_l$) [31] and the parameter γ ($=T_g/(T_g + T_l)$) [32] can be calculated accordingly to estimate the GFA of these ribbons. The T_{rg} and γ are about 0.451 and 0.354 for $x = 5$, 0.483 and 0.358 for $x = 6$, and 0.485 and 0.362 for $x = 7$, respectively. Both the T_{rg} and γ increase with the increase of boron content, which indicates that the addition of boron can improve the GFA of the $\text{Fe}_{87}\text{Ce}_{13-x}\text{B}_x$ ($x = 5, 6, 7$) MG ribbons.

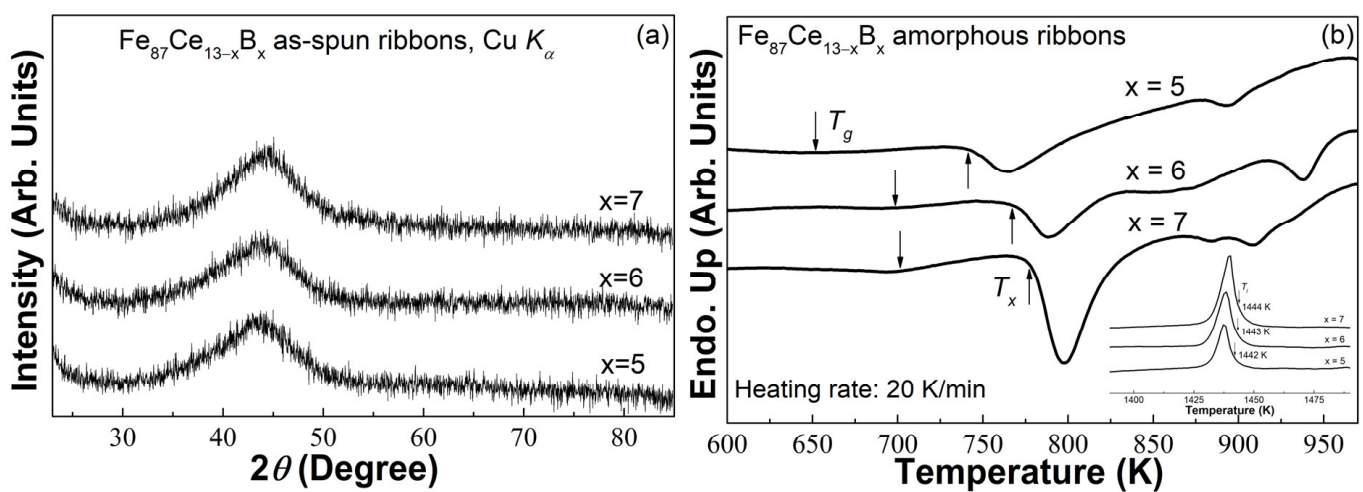


Figure 1. (a) The XRD patterns of the $\text{Fe}_{87}\text{Ce}_{13-x}\text{B}_x$ ($x = 5, 6, 7$) as-spun ribbons; (b) the DSC traces of the $\text{Fe}_{87}\text{Ce}_{13-x}\text{B}_x$ ($x = 5, 6, 7$) amorphous ribbons at the heating rate of 20 K/min; the inset is the melting behaviors.

Table 1. The thermal properties and magnetic properties of the $\text{Fe}_{87}\text{Ce}_{13-x}\text{B}_x$ ($x = 5, 6, 7$) amorphous ribbons.

Composition	T_g (K)	T_x (K)	T_l (K)	T_{rg}	γ	T_c (K)
$x = 5$	651	741	1442	0.451	0.354	283
$x = 6$	698	767	1443	0.483	0.358	305
$x = 7$	701	777	1444	0.485	0.362	323
	$-\Delta S_m^{\text{peak}}$ (J/(kg × K))					
	1 T	1.5 T	2 T	3 T	4 T	5 T
$x = 5$	1.08	1.48	1.84	2.49	3.09	3.66
$x = 6$	1.14	1.56	1.94	2.63	3.28	3.88
$x = 7$	1.12	1.52	1.89	2.56	3.17	3.75

The hysteresis loops at 180 K and 380 K of the $\text{Fe}_{87}\text{Ce}_{13-x}\text{B}_x$ ($x = 5, 6, 7$) glassy ribbons were measured under the maximum field of 5 T, as shown in Figure 2a–c. All glassy ribbons are paramagnetic at 380 K and soft magnetic with near zero hystereses at 180 K, which suggests that these ribbons transform from ferromagnetism to paramagnetism between 180 K and 380 K. The saturation magnetizations (M_s) at 180 K of the three samples are about 129.4 Am²/kg, 143.2 Am²/kg, and 142.1 Am²/kg, respectively. The M_s first increases and then slightly decreases with the boron content. To determine the ferromagnetic–paramagnetic transition temperature of the $\text{Fe}_{87}\text{Ce}_{13-x}\text{B}_x$ ($x = 5, 6, 7$) MG ribbons, we

measured their M - T curves from 180 K to 380 K under 0.03 T after cooling these samples without any applied fields. As illustrated in the insets of Figure 2a–c, all M - T curves of the $\text{Fe}_{87}\text{Ce}_{13-x}\text{B}_x$ ($x = 5, 6, 7$) ribbons show similar shapes, and T_c can be deduced to be ~ 283 K for $x = 5$, ~ 305 K for $x = 6$, and ~ 323 K for $x = 7$, respectively. It was found that T_c of the $\text{Fe}_{87}\text{Ce}_{13-x}\text{B}_x$ ($x = 5, 6, 7$) ribbons almost linearly increases with the increase of boron content. The Curie temperature of the $\text{Fe}_{87}\text{Ce}_{13-x}\text{B}_x$ ($x = 5, 6, 7$) glassy ribbons should also be decided by the interaction between Fe atoms because of only one electron in the $4f$ shell of the Ce atom. The monotonically increasing relationship between T_c and composition was also observed in the Fe-Zr-B ternary amorphous ribbons, which is believed to be due to the enhanced $3d$ - $3d$ direct interaction between Fe atoms by the addition of boron [18,24]. In addition, the increase of boron content (namely the reduction of Ce content) will diminish the antiferromagnetic coupling between Ce and Fe atoms, which can dilute the direct interaction between Fe atoms [30] and, thus, result in the enhancement of $3d$ - $3d$ interaction between Fe atoms.

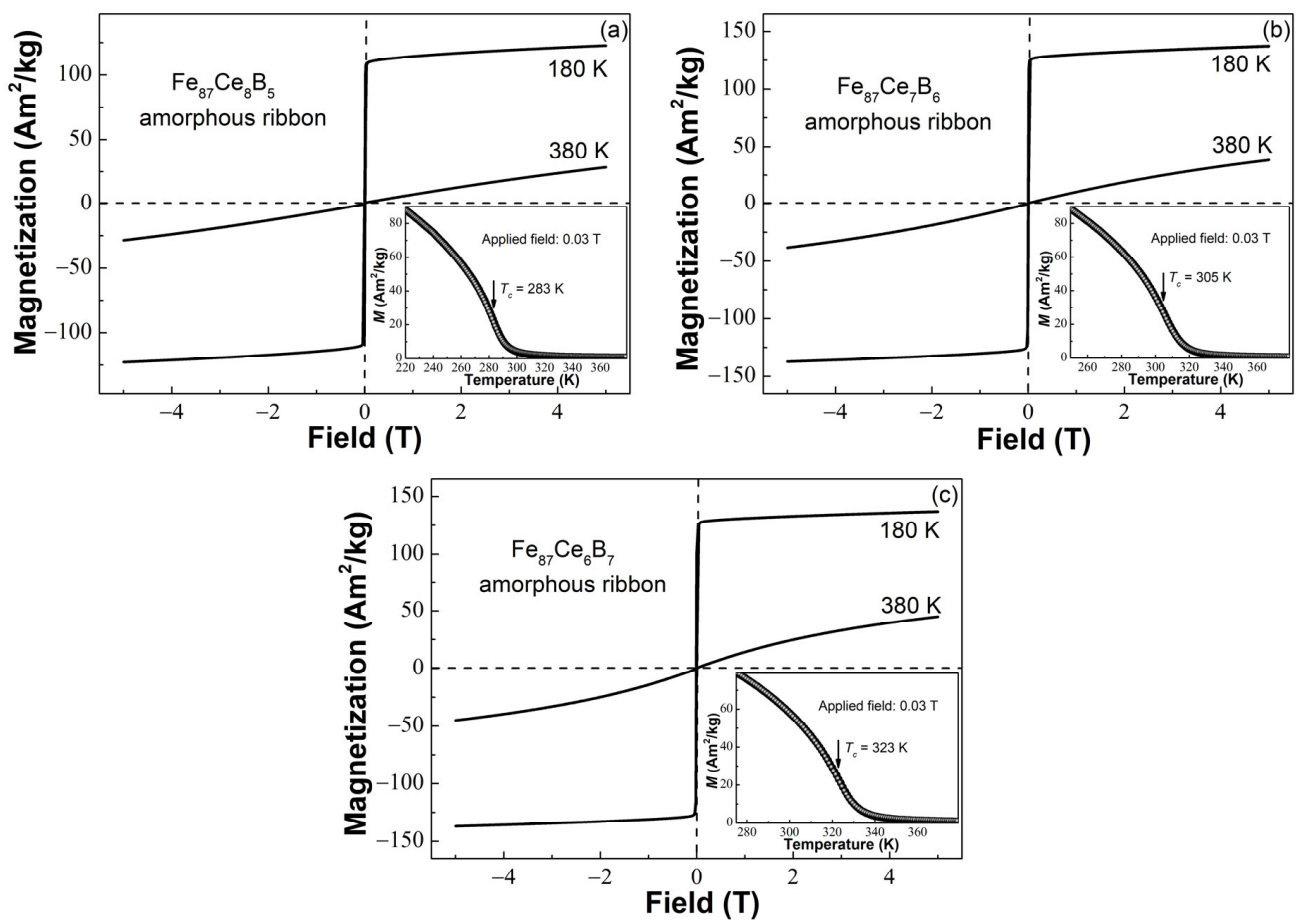


Figure 2. The hysteresis loops of the (a) $\text{Fe}_{87}\text{Ce}_8\text{B}_5$, (b) $\text{Fe}_{87}\text{Ce}_7\text{B}_6$, and (c) $\text{Fe}_{87}\text{Ce}_6\text{B}_7$ amorphous ribbons measured at 180 K and 380 K under 5 T; the insets are their M - T curves measured under 0.03 T.

The Arrott plots can be deduced from their isothermal magnetization curves (not present in the paper) to judge the types of magnetic transition in the $\text{Fe}_{87}\text{Ce}_{13-x}\text{B}_x$ ($x = 5, 6, 7$) amorphous ribbons, as illustrated in Figure 3a–c. The slope of each Arrott plot at every temperature is positive, without “S” or “C”-shaped feature, indicating that both the three alloys experience a second-order ferromagnetic–paramagnetic transition near their T_c [33].

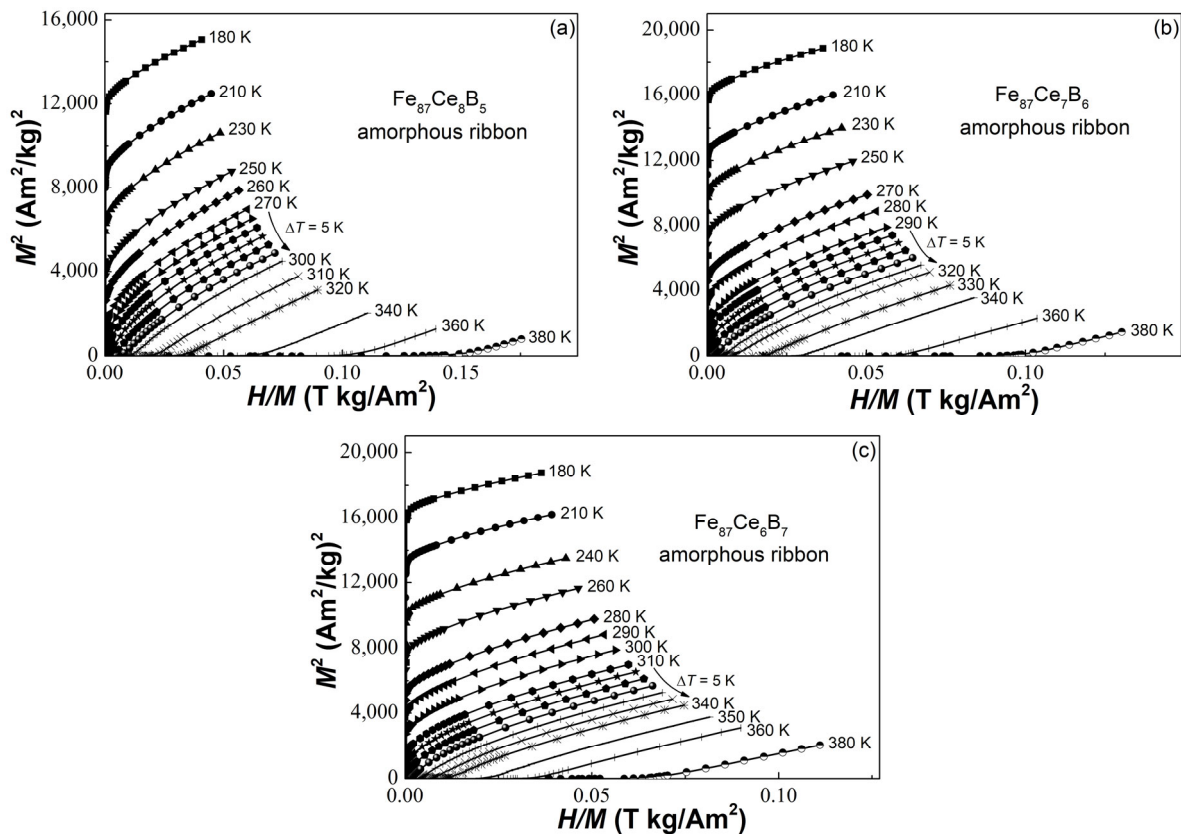


Figure 3. The Arrott plots of the (a) $\text{Fe}_{87}\text{Ce}_8\text{B}_5$, (b) $\text{Fe}_{87}\text{Ce}_7\text{B}_6$, and (c) $\text{Fe}_{87}\text{Ce}_6\text{B}_7$ amorphous ribbons.

In order to characterize MCE of the second-order phase transition $\text{Fe}_{87}\text{Ce}_{13-x}\text{B}_x$ ($x = 5, 6, 7$) amorphous ribbons, the magnetic entropy change can be calculated by Maxwell equation [34]:

$$\Delta S_m(T, H) = S_m(T, H) - S_m(T, 0) = \int_0^H \left(\frac{\partial M}{\partial T} \right)_H dH \quad (1)$$

Figure 4a shows the temperature dependence of $-\Delta S_m$ ($-\Delta S_m$ - T curves) for the $\text{Fe}_{87}\text{Ce}_{13-x}\text{B}_x$ ($x = 5, 6, 7$) ribbons under the magnetic fields of 1.5 T and 5 T. The broadened distribution of each $-\Delta S_m$ - T curve suggests the typical feature of second-order magnetic transition materials. The $-\Delta S_m^{\text{peak}}$ under 1.5 T and 5 T of the $\text{Fe}_{87}\text{Ce}_{13-x}\text{B}_x$ ($x = 5, 6, 7$) ribbons are summarized in Table 1. We can find that the value of $-\Delta S_m^{\text{peak}}$ first increases and then decreases with the increase of boron content and reaches a maximum value of $\sim 3.88 \text{ J}/(\text{kg} \times \text{K})$ under 5 T at $x = 6$. The variation is the same as that in M_s . Although the B substitution for Ce can improve the $3d$ - $3d$ interaction between Fe atoms, which is beneficial for the enhancement of $-\Delta S_m^{\text{peak}}$, the decrease of the Ce atom simultaneously reduces the total magnetic entropy of the alloy, thus resulting in the reduction of $-\Delta S_m^{\text{peak}}$, as the Ce atom also contributes to the magnetic entropy change [18,24,30]. It may be precisely the two opposing factors that lead to this variation in M_s and $-\Delta S_m^{\text{peak}}$. According to the $-\Delta S_m^{\text{peak}}$ under various magnetic fields, the field dependence of $-\Delta S_m^{\text{peak}}$ for the $\text{Fe}_{87}\text{Ce}_{13-x}\text{B}_x$ ($x = 5, 6, 7$) ribbons can be investigated by constructing the $\ln(-\Delta S_m^{\text{peak}})$ - $\ln(H)$ plots, as shown in Figure 4b. Each set of point plots is linearly fitted well, and the slope (expressed by n) of the linear fitting is 0.756 for $x = 5$, 0.759 for $x = 6$, and 0.750 for $x = 7$, respectively. The values of n are consistent with that of other MGs [16–18,23–26,29,30] but slightly larger than the predicted value of the mean field model [35]. This deviation is mainly caused by local inhomogeneity in MGs because the presence of short-range ordered clusters in MGs leads to a magnetic transformation in a wide temperature range [17].

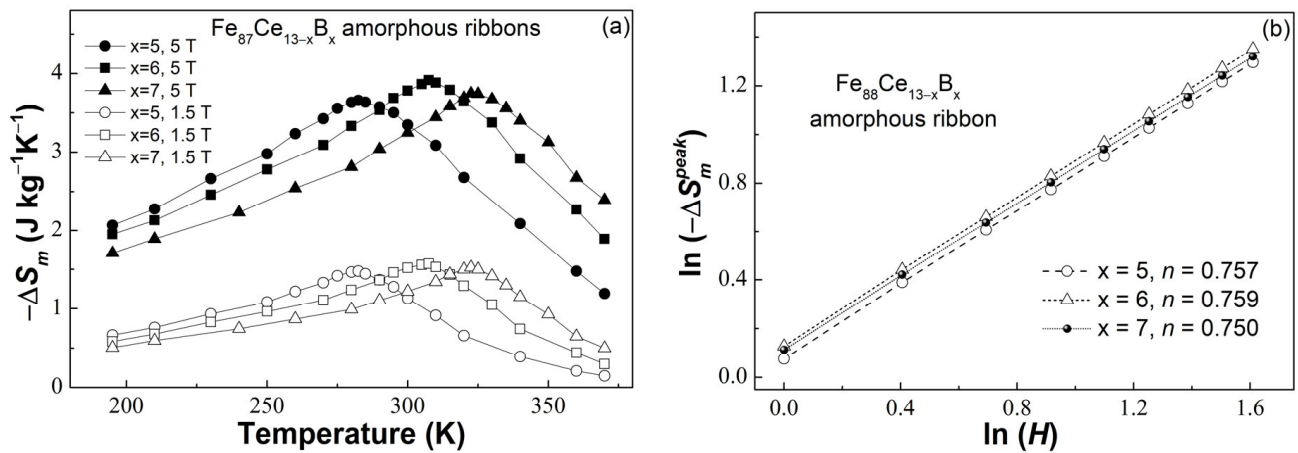


Figure 4. (a) The $(-\Delta S_m)$ - T curves of the Fe₈₇Ce_{13-x}B_x ($x = 5, 6, 7$) amorphous ribbons under 1.5 T and 5 T; (b) the $\ln(-\Delta S_m^{peak})$ vs. $\ln(H)$ plots and their linear fittings of the Fe₈₇Ce_{13-x}B_x ($x = 5, 6, 7$) amorphous ribbons.

Figure 5a displays the $-\Delta S_m^{peak}$ under 5 T of the Fe₈₇Ce_{13-x}B_x ($x = 5, 6, 7$) amorphous ribbons and some Fe-Zr-B-based MGs [15–18,23–26,36]. A positive correlation between $-\Delta S_m^{peak}$ and T_c was observed in the Fe-Zr-B-based MGs, implying that the higher $-\Delta S_m^{peak}$ can only be achieved at higher temperatures for the Fe-Zr-B-based MGs, which is very unfriendly for the application of magnetic refrigeration at room temperature. However, the novel Fe₈₇Ce_{13-x}B_x ($x = 5, 6, 7$) amorphous ribbons prepared in this work provide a better idea and exhibit better magnetocaloric performance than the Fe-Zr-B-based MGs. For example, the lowest $-\Delta S_m^{peak}$ in these amorphous ribbons (~ 3.66 J/(kg \times K) at 282.5 K for Fe₈₇Ce₈B₅) is still 3.1% higher than the largest $-\Delta S_m^{peak}$ in the Fe-Zr-B-based MGs (~ 3.55 J/(kg \times K), while T_c reaches around 335 K [15,25]). The Fe₈₇Ce₇B₆ ribbon with the largest $-\Delta S_m^{peak}$ shows a value at least 9.3% higher than that of the Fe-Zr-B-based MGs. Additionally, the $-\Delta S_m^{peak}$ of the Fe₈₇Ce_{13-x}B_x ($x = 5, 6, 7$) amorphous ribbons is much higher than that of the Fe-Zr-B-based MGs with the same T_c , which can be intuitively observed from Figure 5a.

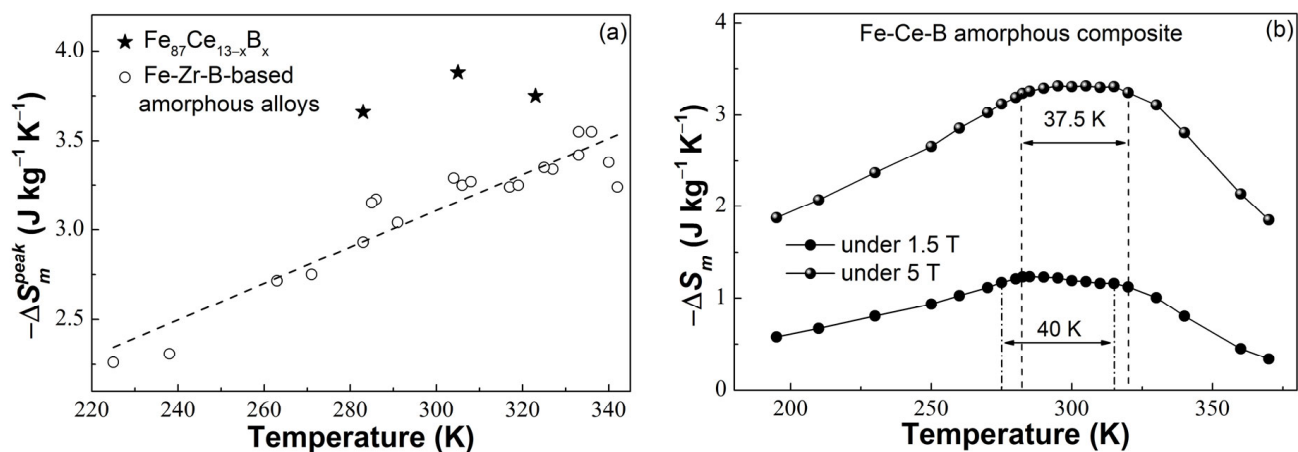


Figure 5. (a) The $-\Delta S_m^{peak}$ of the Fe₈₇Ce_{13-x}B_x ($x = 5, 6, 7$) amorphous ribbons and some Fe-Zr-B-based amorphous alloys under 5 T; (b) the flattened $(-\Delta S_m)$ - T curves of the amorphous composite composed of the three amorphous ribbons under 1.5 T and 5 T.

On the other hand, the T_c of the Fe₈₇Ce_{13-x}B_x ($x = 5, 6, 7$) amorphous ribbons increases from 283 K to 323 K, which perfectly matches the temperature interval of a domestic magnetic refrigeration appliance. Therefore, we can construct an amorphous composite

with a flattened $-\Delta S_m$ profile that is the requirement of application in an Ericsson cycle according to the three ribbons [37]. The $-\Delta S_m$ of the composite can be calculated as follows:

$$-\Delta S_m(\text{composite}) = \sum_{i=1,2,\dots,n}^n w_i \times (-\Delta S_m)_i \quad (2)$$

where w_i is the weight fraction of each component; the validity of Equation (2) has been verified in Ref. [38]. Therefore, by adjusting the weight fraction of these ribbons according to Equation (2), the amorphous composite was designed to be synthesized with 44% (wt.%) $\text{Fe}_{87}\text{Ce}_8\text{B}_5$ + 3% (wt.%) $\text{Fe}_{87}\text{Ce}_7\text{B}_6$ + 53% (wt.%) $\text{Fe}_{87}\text{Ce}_6\text{B}_7$ amorphous ribbons. As shown in Figure 5b, the $-\Delta S_m$ of the amorphous composite fluctuates with an average value of ~ 1.20 J/(kg \times K) from 275 K to 315 K ($\Delta T_{\text{table}} = 40$ K) under 1.5 T, and ~ 3.29 J/(kg \times K) from 282.5 K to 320 K ($\Delta T_{\text{table}} = 37.5$ K) under 5 T. Compared with the Fe-Zr-B-based amorphous composite materials, an amorphous hybrid with a larger average $-\Delta S_m$ ($-\Delta S_m^{\text{average}}$) was achieved in this work [15–17]. In addition, the effective cooling capacity ($RC_{\text{eff}} = -\Delta S_m^{\text{average}} \times \Delta T_{\text{table}}$ [39]) used to assess the actual cooling capacity of the Fe-Ce-B amorphous hybrid was calculated to be about 48.0 J/kg under 1.5 T and 123.4 J/kg under 5 T, both of which are also higher than those of the Fe-Zr-B-based amorphous composites with a similar ΔT_{table} [15,17,39]. Furthermore, considering that the components of the amorphous composite do not contain radioactive elements, the Fe-Ce-B amorphous hybrid, thereby, shows a better application potential as highly efficient refrigerants in a domestic magnetic refrigeration appliance.

4. Conclusions

In summary, we successfully prepared the $\text{Fe}_{87}\text{Ce}_{13-x}\text{B}_x$ ($x = 5, 6, 7$) amorphous ribbons, and the influences of boron addition on their GFA, T_c , and $-\Delta S_m^{\text{peak}}$ were systematically investigated. The main conclusions are as follows:

- (i) The T_{rg} and γ indicate that the GFA of the $\text{Fe}_{87}\text{Ce}_{13-x}\text{B}_x$ ($x = 5, 6, 7$) ribbons were increased with the addition of boron;
- (ii) All ribbons show soft magnetic properties with negligible coercivity at 180 K, and T_c of the $\text{Fe}_{87}\text{Ce}_{13-x}\text{B}_x$ ($x = 5, 6, 7$) amorphous ribbons is ~ 283 K for $x = 5$, ~ 305 K for $x = 6$, and ~ 323 K for $x = 7$, respectively. The increased T_c with the addition of boron may be due to the enhanced $3d-3d$ interaction between Fe atoms induced by the increase of boron content and the reduction of Ce content;
- (iii) The $-\Delta S_m^{\text{peak}}$ of the $\text{Fe}_{87}\text{Ce}_{13-x}\text{B}_x$ ($x = 5, 6, 7$) amorphous ribbons first increases and subsequently decreases with the increase of boron content, which is supposed to be related to the competitive effect between the enhanced $3d-3d$ interaction by the addition of B content and the reduced total magnetic entropy by the decrease of Ce content;
- (iv) Both Arrott plots and the value of n at T_c suggest the typical second-order magnetic transition magnetocaloric behavior of the three ribbons. All the $\text{Fe}_{87}\text{Ce}_{13-x}\text{B}_x$ ($x = 5, 6, 7$) amorphous ribbons show rather excellent MCE than Fe-Zr-B-based metallic glasses.

Based on the above results, we designed an amorphous composite with a flattened ($-\Delta S_m$)- T curve by using 44% (wt.%) $\text{Fe}_{87}\text{Ce}_8\text{B}_5$ + 3% (wt.%) $\text{Fe}_{87}\text{Ce}_7\text{B}_6$ + 53% (wt.%) $\text{Fe}_{87}\text{Ce}_6\text{B}_7$ ribbons. The high $-\Delta S_m^{\text{average}}$ (~ 3.29 J/(kg \times K)) and RC_{eff} (~ 123.4 J/kg) from 282.5 K to 320 K under 5 T indicate that the hybrid is a promising candidate as a refrigerant applied in a domestic magnetic refrigeration appliance.

Author Contributions: Conceptualization, L.X., P.Y. and J.-L.Y.; methodology, D.D.; validation, Q.W. and B.-Z.T.; investigation, S.-H.Z., L.-Z.Z. and P.-J.W.; data curation, Q.W., S.-H.Z. and B.-Z.T.; writing—original draft preparation, S.-H.Z. and Q.W.; writing—review and editing, L.X.; funding acquisition, L.X. and P.Y. All authors have read and agreed to the published version of the manuscript.

Funding: This research was funded by the National Natural Science Foundation of China, grant numbers 51871139, 52071196, and 52071043.

Institutional Review Board Statement: Not applicable.

Informed Consent Statement: Not applicable.

Data Availability Statement: Data sharing is not applicable.

Acknowledgments: This research was technically supported by the Center for Advanced Microanalysis of Shanghai University.

Conflicts of Interest: The authors declare no conflict of interest in this work.

References

1. Chaudhary, V.; Chen, X.; Ramanujan, R.V. Iron and manganese based magnetocaloric materials for near room temperature thermal management. *Prog. Mater. Sci.* **2019**, *100*, 64–98. [[CrossRef](#)]
2. Bruck, E. Developments in magnetocaloric refrigeration. *J. Phys. D. Appl. Phys.* **2005**, *38*, R381–R391. [[CrossRef](#)]
3. de Oliveira, N.A.; von Ranke, P.J. Theoretical aspects of the magnetocaloric effect. *Phys. Rep.* **2010**, *489*, 89–159. [[CrossRef](#)]
4. Franco, V.; Blázquez, J.S.; Ipus, J.J.; Law, J.Y.; Moreno-Ramírez, L.M.; Conde, A. Magnetocaloric effect: From materials research to refrigeration devices. *Prog. Mater. Sci.* **2018**, *93*, 112–232. [[CrossRef](#)]
5. Gschneidner, K.A., Jr.; Pecharsky, V.K. Magnetocaloric Materials. *Annu. Rev. Mater. Sci.* **2000**, *30*, 387–429. [[CrossRef](#)]
6. Giauque, W.F.; Macdougall, D.P. Attainment of temperature below 1° absolute by demagnetization of $\text{Gd}_2(\text{SO}_4)_3 \cdot 8\text{H}_2\text{O}$. *Phys. Rev.* **1933**, *43*, 768. [[CrossRef](#)]
7. Shen, B.G.; Sun, J.R.; Hu, F.X.; Zhang, H.W.; Cheng, Z.H. Recent Progress in Exploring Magnetocaloric Materials. *Adv. Mater.* **2009**, *21*, 4545–4564. [[CrossRef](#)]
8. Pecharsky, V.K.; Gschneidner, K.A., Jr. Tunable magnetic regenerator alloys with a giant magnetocaloric effect for magnetic refrigeration from ~20 to ~290 K. *Appl. Phys. Lett.* **1997**, *70*, 3299–3301. [[CrossRef](#)]
9. Pecharsky, V.K.; Gschneidner, K.A., Jr. Giant magnetocaloric effect in $\text{Gd}_5(\text{Si}_2\text{Ge}_2)$. *Phys. Rev. Lett.* **1997**, *78*, 4494–4497. [[CrossRef](#)]
10. Miao, X.F.; Wang, W.Y.; Liang, H.X.; Qian, F.J.; Cong, M.Q.; Zhang, Y.J.; Muhammad, A.; Tian, Z.J.; Xu, F. Printing (Mn,Fe)₂(P,Si) magnetocaloric alloys for magnetic refrigeration applications. *J. Mater. Sci.* **2020**, *55*, 6660–6668. [[CrossRef](#)]
11. Pasquale, M.; Sasso, C.P.; Lewis, L.H.; Giudici, L.; Lograsso, T.; Schlagel, D. Magnetostructural transition and magnetocaloric effect in $\text{Ni}_{55}\text{Mn}_{20}\text{Ga}_{25}$ single crystals. *Phys. Rev. B* **2005**, *72*, 094435. [[CrossRef](#)]
12. Hashimoto, T.; Kuzuhara, T.; Sahashi, M.; Inomata, K.; Tomokiyo, A.; Yayama, H. New application of complex magnetic materials to the magnetic refrigerant in an Ericsson magnetic refrigerator. *J. Appl. Phys.* **1987**, *62*, 3873–3878. [[CrossRef](#)]
13. Xia, L.; Tang, M.B.; Chan, K.C.; Dong, Y.D. Large magnetic entropy change and adiabatic temperature rise of a $\text{Gd}_{55}\text{Al}_{20}\text{Co}_{20}\text{Ni}_5$ bulk metallic glass. *J. Appl. Phys.* **2014**, *115*, 223904. [[CrossRef](#)]
14. Bingham, N.S.; Wang, H.; Qin, F.; Peng, H.X.; Sun, J.F.; Franco, V.; Srikanth, H.; Phan, M.H. Excellent magnetocaloric properties of melt-extracted Gd-based amorphous microwires. *Appl. Phys. Lett.* **2012**, *101*, 102407. [[CrossRef](#)]
15. Chen, L.S.; Zhang, J.Z.; Wen, L.; Yu, P.; Xia, L. Outstanding magnetocaloric effect of $\text{Fe}_{88-x}\text{Zr}_8\text{B}_4\text{Sm}_x$ ($x=0, 1, 2, 3$) amorphous alloys. *Sci. China. Phys. Mech. Astron.* **2018**, *61*, 056121. [[CrossRef](#)]
16. Gan, L.H.; Ma, L.Y.; Tang, B.Z.; Ding, D.; Xia, L. Effect of Co substitution on the glass forming ability and magnetocaloric effect of $\text{Fe}_{88}\text{Zr}_8\text{B}_4$ amorphous alloys. *Sci. China. Phys. Mech. Astron.* **2017**, *60*, 076121. [[CrossRef](#)]
17. Peng, J.X.; Tang, B.Z.; Wang, Q.; Bai, C.; Wu, Y.; Chen, Q.X.; Li, D.M.; Ding, D.; Xia, L.; Guo, X.L.; et al. Effect of heavy rare-earth (Dy, Tb, Gd) addition on the glass-forming ability and magneto-caloric properties of $\text{Fe}_{89}\text{Zr}_7\text{B}_4$ amorphous alloy. *J. Alloys Compd.* **2022**, *925*, 166707. [[CrossRef](#)]
18. Yu, P.; Zhang, J.Z.; Xia, L. Effect of boron on the magneto-caloric effect in $\text{Fe}_{91-x}\text{Zr}_9\text{B}_x$ ($x = 3, 4, 5$) amorphous alloys. *J. Mater. Sci.* **2017**, *52*, 13948–13955. [[CrossRef](#)]
19. Waske, A.; Schwarz, B.; Mattern, N.; Eckert, J. Magnetocaloric (Fe-B)-based amorphous alloys. *J. Magn. Magn. Mater.* **2013**, *329*, 101–104. [[CrossRef](#)]
20. Zhang, M.X.; Li, J.W.; Kong, F.L.; Liu, J. Magnetic properties and magnetocaloric effect of FeCrNbYB metallic glasses with high glass-forming ability. *Intermetallics* **2015**, *59*, 18–22. [[CrossRef](#)]
21. Caballero-Flores, R.; Franco, V.; Conde, A.; Kiss, L.F. Influence of Mn on the magnetocaloric effect of nanoperm-type alloys. *J. Appl. Phys.* **2010**, *108*, 073921. [[CrossRef](#)]
22. Min, S.G.; Kim, K.S.; Yu, S.C.; Lee, K.W. The magnetization behavior and magnetocaloric effect in amorphous Fe-Nb-B ribbons. *Mater. Sci. Eng. A-Struct. Mater. Prop. Microstruct. Process.* **2007**, *449*, 423–425. [[CrossRef](#)]
23. Wang, X.; Wang, Q.; Tang, B.Z.; Ding, D.; Cui, L.; Xia, L. Effect of Mn Substitution Fe on the Formability and Magnetic Properties of Amorphous $\text{Fe}_{88}\text{Zr}_8\text{B}_4$ Alloy. *Metals* **2021**, *11*, 1577. [[CrossRef](#)]
24. Wang, X.; Wang, Q.; Tang, B.Z.; Ding, D.; Cui, L.; Xia, L. Magnetic and Magneto-Caloric Properties of the Amorphous $\text{Fe}_{92-x}\text{Zr}_8\text{B}_x$ Ribbons. *Materials* **2020**, *13*, 5334. [[CrossRef](#)]
25. Wu, Y.B.; Wang, Q.; Tang, B.Z.; Pan, L.L.; Ding, D.; Xia, L. Outstanding glass formability and magneto-caloric effect of a $\text{Fe}_{85}\text{Co}_3\text{Zr}_5\text{B}_4\text{Nb}_3$ metallic glass. *J. Non-Cryst. Solids* **2021**, *566*, 120885. [[CrossRef](#)]
26. Yu, P.; Zhang, J.Z.; Xia, L. $\text{Fe}_{87}\text{Zr}_7\text{B}_4\text{Co}_2$ amorphous alloy with excellent magneto-caloric effect near room temperature. *Intermetallics* **2018**, *95*, 85–88. [[CrossRef](#)]

27. Li, H.X.; Lu, Z.C.; Wang, S.L.; Wu, Y.; Lu, Z.P. Fe-based bulk metallic glasses: Glass formation, fabrication, properties and applications. *Prog. Mater. Sci.* **2019**, *103*, 235–318. [[CrossRef](#)]
28. Inoue, A.; Takeuchi, A. Recent development and application products of bulk glassy alloys. *Acta Mater.* **2011**, *59*, 2243–2267. [[CrossRef](#)]
29. Wang, C.H.; Wang, Q.; Tang, B.Z.; Zhou, X.; Ding, D.; Xia, L. Achieve good magneto-caloric response near the ambient temperature in a $\text{Fe}_{86}\text{La}_7\text{B}_5\text{Ce}_2$ amorphous ribbon. *J. Magn. Magn. Mater.* **2022**, *547*, 168954. [[CrossRef](#)]
30. Li, A.L.; Wang, Q.; Tang, B.Z.; Yu, P.; Ding, D.; Xia, L. Magnetocaloric effect of the $\text{Fe}_{87}\text{M}_8\text{B}_5$ ($\text{M} = \text{Zr}, \text{Ce}$) amorphous alloys. *Mater. Sci. Eng. B-Adv.* **2022**, *286*, 116033. [[CrossRef](#)]
31. Turnbull, D. Under what conditions can a glass be formed? *Contemp. Phys.* **1969**, *10*, 473–488. [[CrossRef](#)]
32. Lu, Z.P.; Liu, C.T. A new glass-forming ability criterion for bulk metallic glasses. *Acta Mater.* **2002**, *50*, 3501–3512. [[CrossRef](#)]
33. Banerjee, S.K. On a generalized approach to first and second order magnetic transitions. *Phys. Lett.* **1964**, *12*, 16–17. [[CrossRef](#)]
34. Hashimoto, T.; Numasawa, T.; Shino, M.; Okada, T. Magnetic refrigeration in the temperature range from 10 K to room temperature: The ferromagnetic refrigerants. *Cryogenics* **1981**, *21*, 647–653. [[CrossRef](#)]
35. Oesterreicher, H.; Parker, F.T. Magnetic cooling near Curie temperatures above 300 K. *J. Appl. Phys.* **1984**, *55*, 4334–4338. [[CrossRef](#)]
36. Zheng, X.N.; Wang, Q.; Yue, C.Y.; Li, A.L.; Ding, D.; Xia, L. Achieving higher magnetic entropy change peak at lower temperature by minor Ti substitution for Zr in the $\text{Fe}_{88}\text{Zr}_8\text{B}_4$ metallic glass. *Mod. Phys. Lett. B* **2023**, *37*, 2350032. [[CrossRef](#)]
37. Smaili, A.; Chahine, R. Composite materials for Ericsson-like magnetic refrigeration cycle. *J. Appl. Phys.* **1997**, *81*, 824. [[CrossRef](#)]
38. Ma, L.Y.; Gan, L.H.; Chan, K.C.; Ding, D.; Xia, L. Achieving a table-like magnetic entropy change across the ice point of water with tailorable temperature range in Gd-Co-based amorphous hybrids. *J. Alloys Compd.* **2017**, *723*, 197–200. [[CrossRef](#)]
39. Álvarez, P.; Gorria, P.; Llamazares, J.L.S.; Blanco, J.A. Searching the conditions for a table-like shape of the magnetic entropy in magneto-caloric materials. *J. Alloys Compd.* **2013**, *568*, 98–101. [[CrossRef](#)]

Disclaimer/Publisher's Note: The statements, opinions and data contained in all publications are solely those of the individual author(s) and contributor(s) and not of MDPI and/or the editor(s). MDPI and/or the editor(s) disclaim responsibility for any injury to people or property resulting from any ideas, methods, instructions or products referred to in the content.